Letter

Spatiotemporal dynamics of particle collisions in quantum spin chains

P. I. Karpov [1,2,*] G.-Y. Zhu [1,†] M. P. Heller [3,4,‡] and M. Heyl [1,§]

[1]*Max Planck Institute for the Physics of Complex Systems, 01187 Dresden, Germany*

[2]*Arnold Sommerfeld Center for Theoretical Physics, Ludwig Maximilian University of Munich, Theresienstrasse 37, 80333 Munich, Germany*

[3]*Max Planck Institute for Gravitational Physics (Albert Einstein Institute), 14476 Potsdam, Germany*

[4]*Department of Physics and Astronomy, Ghent University, 9000 Ghent, Belgium*

(Received 10 December 2020; revised 25 October 2021; accepted 14 March 2022; published 1 July 2022)

We show that quantum Ising chains provide a platform to realize and probe elastic and inelastic particle collisions in pristine form. The proposed setup allows us to monitor the whole spatiotemporal dynamics of the collision event. The considered Ising chains admit a natural realization in various quantum simulator platforms, and we discuss a potentially feasible implementation of our collision protocol in Rydberg atoms. We also argue that the results and techniques we introduce can be readily extended to lattice gauge theories and to a higher number of spatial dimensions.

DOI: 10.1103/PhysRevResearch.4.L032001

Introduction and summary. Quantum simulator platforms have seen tremendous progress within the past two decades in controlling and probing the real-time dynamics of quantum matter [1–3]. A long-standing goal in the field has been the realization of lattice gauge theories (LGTs) [4–10] with the associated confinement phenomena. The underlying long-term perspective has been to address fundamental dynamical real-time phenomena of high-energy physics in the presence of confinement [11–22], in particular string breaking [23], false vacuum decay [24], or particle collisions [25]. The newest developments in programmable quantum simulators such as Rydberg atoms have highlighted the potential to access new physical regimes of quantum spin models [26–34], which have remained elusive so far.

Motivated by this progress, we propose and validate a collision protocol in quantum spin models [35], which has four key advantages. First, the protocol is versatile and controllable, making a wealth of dynamical phenomena accessible, including various patterns of particle production. Second, it allows for monitoring spatiotemporal dynamics throughout the whole collision event *in situ*, not only asymptotic states. Third, it lies within reach of current quantum simulation platforms. Fourth, the protocol admits an efficient theoretical description that can solve the resulting quantum dynamics with computation effort only polynomial with volume. This makes it directly applicable also to higher spatial dimensions.

Concretely, we explore the dynamics generated by quantum Ising chains, where confinement of domain walls can be induced by longitudinal fields [15]. The resulting bound states—mesons—provide natural particle projectiles [36,37]. Our collision protocol is initiated with two mesonic wave

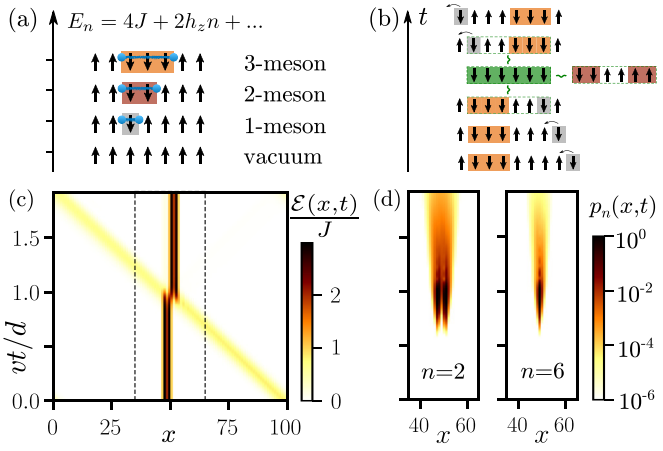

FIG. 1. (a) Low-energy states of the Ising chain: domain walls (blue dots) separated by n sites are confined in pairs ("n-mesons") due to a linear interaction potential $E_n \sim h_z n$. (b) Schematic illustration of the $(3+1)$-collision of a 3-meson with a 1-meson for $h_z = J$ highlighting the formation of intermediate 6- and 2-mesons. (c), (d) Spatiotemporal picture of the $(3+1)$-collision for an initial distance d and a 1-meson wave packet with momentum $k = \pi/2$ and velocity $v = 2h_x^2/3J$. (c) Local energy $\mathcal{E}(x,t)$. (d) Spatially resolved meson occupations $p_n(x,t)$ for $n = 2$ (left) and $n = 6$ (right). The data are obtained for a chain of $L = 100$ sites within the effective model (2)–(5).

*karpov@pks.mpg.de

†guoyi@pks.mpg.de

‡On leave from: National Centre for Nuclear Research, Warsaw 02093, Poland; michal.p.heller@aei.mpg.de

§heyl@pks.mpg.de

packets impacting onto each other; see Fig. 1. We show that our setup not only allows us to realize simple elastic collisions, but also inelastic ones with intricate particle production patterns that can be spatiotemporally resolved via simple measurements; see Figs. 2 and 3. Regarding quantum simulation prospects, we discuss a potential implementation, see Fig. 4, and its feasibility in the context of Rydberg atoms [26–34]. Finally, we discuss how our approach can be extended to general LGTs. This covers also the case of higher spatial dimensions, where quantum dynamics is even more challenging.

Setup. We consider the quantum Ising chain with transverse h_x and longitudinal h_z fields

$$H = -J\sum_{i=1}^{L}\sigma_i^z\sigma_{i+1}^z - h_x\sum_{i=1}^{L}\sigma_i^x - h_z\sum_{i=1}^{L}\sigma_i^z, \qquad (1)$$

where $\sigma_i^{x(z)}$ denotes the Pauli matrix at site i in a periodic chain of L sites. The presence of the longitudinal field splits the otherwise degenerate Ising vacuum in the ferromagnetic phase with the central consequence that two domain walls now experience an interaction potential increasing linearly as a function of their distance [15] leading to their confinement. The low-lying excitations are bound states of two domain walls, connected by an electric string with energy proportional to the string length [Fig. 1(a)]. The Ising model can be mapped to a $\mathbb{Z}_2$ LGT with σ_j^z as the electric field and $\mathbb{Z}_2$ matter charges at each domain wall [22]. Therefore, our analysis applies to the broader context of LGTs.

For the purpose of obtaining full spatiotemporal resolution of collisions, we focus on the weak transverse field limit, $h_x \ll J$. We derive an effective description in terms of the aforementioned mesons by defining hard-core bosonic operators $\psi_x^{[n]\dagger} = P^{\uparrow}_{x+[n/2]-n}\prod_{j=x+[n/2]-n+1}^{x+[n/2]}\sigma_j^- P^{\uparrow}_{x+[n/2]+1}$ with $P_j^{\uparrow(\downarrow)} \equiv (1\pm\sigma_j^z)/2$ the projector onto $\uparrow$ ($\downarrow$) at site j. By means of a Schrieffer-Wolff (SW) transformation [38] applied to (1) for weak h_x we arrive at

$$H_{\rm eff} = H_0 + H_{\rm int}, \qquad (2)$$

where H_0 for the case of our main focus, $h_z \simeq J$, reads

$$H_0 = \sum_{n,x} m_n p_n(x) - \frac{v}{2}\sum_x\left(\psi_x^{[1]\dagger}\psi_{x+1}^{[1]} + \text{H.c.}\right) \qquad (3)$$

and contains both the energies of the n-mesons,

$$m_n = 4J + 2nh_z + (4-n-5\,\delta_{n,1})h_x^2/3J + O\big(h_x^4\big), \qquad (4)$$

and the velocity of the 1-mesons $v = 2h_x^2/3J$. Here $p_n(x) = \psi_x^{[n]\dagger}\psi_x^{[n]}$ denotes the occupation of an n-meson at site x. Other values of h_z would modify the masses and velocities.

Note that the regime explored in the present work, $h_x \ll h_z \simeq J$, is different from the Ising field theory limit $h_z \ll h_x \simeq J$ [36,37,39] experimentally realized in a solid-state setting [40] (see [41] for a discussion comparing these two regimes). Crucially, being far away from the integrable point $h_z = 0, h_x = J$ [39], we can observe inelastic collisions and exotic multimeson bound states, as we shall see below.

In our limit $h_x \ll h_z \simeq J$, only 1-, 2-, and 3-mesons are quasistable particles, i.e., have energies below continuum (band) of 1-meson pairs. For the lightest meson, the Hamiltonian H_0 gives a dispersion relation $\epsilon_k = m_1 - v\cos k + O(h_x^4)$. The heavier n-mesons with $n > 1$ are inert on the timescales $t \ll h_x^4/J^3$ we consider, hence m_n's with $n > 1$ act as rest masses, whereas m_1 includes the maximal kinetic energy of the 1-meson.

Essential for the targeted particle collisions, the mesons exhibit interactions,

$$\begin{aligned} H_{\rm int} = &-\frac{h_x^2}{J}\sum_{m,n,x}\left(\psi_x^{[m+n+2]\dagger}\psi_x^{[m]}\psi_{x+m+2}^{[n]} + \text{H.c.}\right) \\ &+ \frac{h_x^2}{J}\sum_{m,n,x}\left(\psi_x^{[m-1]\dagger}\psi_{x+m}^{[n+1]\dagger}\psi_x^{[m]}\psi_{x+m+1}^{[n]} + \text{H.c.}\right) \\ &+ \frac{3h_x^2}{2J}\sum_{m,n,x}\left(\psi_x^{[m]\dagger}\psi_x^{[m]}\psi_{x+m+1}^{[n]\dagger}\psi_{x+m+1}^{[n]} + \text{H.c.}\right), \end{aligned} \qquad (5)$$

which we displayed for $h_z = J$. The first interaction term describes the fusion of two nearby mesons m and n to a heavier $m+n+2$ one upon converting domain-wall excitations into string energy, or the reverse process (essential for string breaking). The second term describes string exchange between two nearby mesons. The last term is a repulsive nearest-neighbor density-density interaction between two mesons. For general $h_z \neq J$ only slight modifications have to be incorporated in (5), such as h_z-dependent corrections to the coupling constants [41].

The limit $h_x \ll J$ has the advantage that the mesons become spatially localized, allowing us to access the full spatiotemporal resolution of the collision dynamics using *simple* projective measurements. While in the original basis the meson operators are dressed, this dressing is only perturbative in h_x/J. In the limit $h_x/J \to 0$ upon keeping $h_x^2 t/J = \text{const}$ the meson expectation values computed with the full Hamiltonian (1) and the effective one (2)–(5) become identical, see Fig. 2(a), as we study employing exact diagonalization (ED).

We complement these projective observables with the local energy $\mathcal{E}(x,t)$ at site $x \equiv i$ being the SW transformed Ising Hamiltonian density $-J\sigma_i^z(\sigma_{i-1}^z + \sigma_{i+1}^z)/2 - h_x\sigma_i^x - h_z\sigma_i^z$.

Collision protocol. We generate propagating n-mesons in the form of Gaussian wave packets by the operator

$$\psi^{[n]}(x_0,k_0)^\dagger = \frac{1}{\sqrt{\mathcal{N}}}\sum_{x=-\infty}^{\infty} e^{-x^2/(4\tau_x^2)}e^{ik_0x}\prod_{j=0}^{n-1}\sigma^-_{x_0+x+j} \qquad (6)$$

acting on the ferromagnetic background, with τ_x denoting the width and $\mathcal{N}$ the normalization factor. The characteristics of the collision process, however, do not depend on the details for wave packets sufficiently localized in momentum space (to avoid spreading). Concretely, we choose $\tau_x = \sqrt{L/4\pi}$ implying $\tau_k \sim 1/\sqrt{L}$ for the width in momentum space. For the collision we decompose the system into two halves, each containing one of the two colliding particles, and we constrain the summation over x to one-half to avoid overlap of the two initial mesons. In the limit $h_x \ll J$, only the 1-meson can propagate on timescales $t \ll J^3/h_x^4$, see Eq. (3), so that we focus on collisions involving at least one 1-meson, while also collisions with propagating higher-mesons can be realized when addressing longer timescales [41]. We maximize the kinetic energy by considering 1-mesons at maximum group

velocity, choosing $k_0 = \pm\pi/2$. Static higher-n mesons can be prepared by flipping n spins in a ferromagnetic background.

As we discuss below, inelastic collisions of various characters can be realized in the considered model. The creation of new mesons from the kinetic energy can be deduced from mesonic spectra. The simpler case of elastic collisions is presented in [41].

Inelastic collision. For studying inelastic collisions, we focus on a strong-coupling limit $h_z = J \gg h_x$ implying a large string tension, which facilitates identification of resonant channels. For this parameter regime, a state consisting of a 3- and a 1-meson is resonant with both a 6-meson and a state involving two 2-mesons from an analysis of the rest masses in the effective model (2) upon temporarily neglecting the perturbative $(h_x/J)^2$ corrections.

Figure 1(b) displays a collision scheme for a 1-meson incident on the 3-meson. When the target and the projectile are separated by two ↑-spins, a second-order in h_x/J spin-flip process, i.e., the fusion interaction term in (5), maps them to a resonant (based on the estimate of the classical rest masses without h_x/J corrections) 6-meson configuration. The 6-meson can then transform resonantly via a similar process of flipping the two central spins to a state with two 2-mesons or back to a configuration with a 1-meson on the left of a 3-meson (see [41] for other channels).

The spatiotemporal dynamics of $\mathcal{E}(x,t)$ in Fig. 1(c) allows one to identify the shift of the 3-meson during the collision, see Fig. 1(b), which might be viewed as a quantum spin chain analog of Newton's cradle (studied only in bosonic [42,43] and fermionic systems [44,45]). Figure 1(d) shows the space-time particle production of the 6- and 2-mesons during the collision process. After the collision, the 6-meson and a pair of 2-mesons can propagate mediated by the motion of a 1-meson, while gradually decaying back to $(3+1)$-meson states [41].

In Fig. 2 we analyze the individual n-mesons across the collision based on their global occupations $\mathcal{P}_n(t) = \sum_x p_n(x,t)$. Figure 2(a) displays $\mathcal{P}_n(t)$ relative to the initial condition $\mathcal{P}_n(t=0)$ to highlight the changes due to the collision with an additional normalization to the height $p_1^{\max} = \max_x p_1(x, t=0)$ of the incident 1-meson wave packet. With this we eliminate a dependence on the details of the incident wave packet. A wave packet broader in real space will hit the 3-meson only with a reduced maximal amplitude thereby also lowering the particle production at a given time instance. Figure 2(a) compares both data from full ED for Eq. (1) as well as from Eq. (2) for $h_x/J = 10^{-2}$. Collapse of the two datasets confirms the accuracy of Eq. (2), which we will use extensively in the remainder of the paper.

Figure 2(a) shows that the collision is accompanied by a significant production of 2- and 6-mesons [see also Fig. 1(b)]. After the collision, some of the intermediate 2- and 6-mesons convert back to 1- and 3-mesons. Importantly, also an inelastic channel remains as we display in more detail in Fig. 2(b) for 2- and 6-meson occupations on a logarithmic scale. These particles are not just created via some intermediate state but remain also after the collision as the inelastic contributions with a weak decay over time. Note that the time axis in Fig. 2(b) is rescaled by the initial distance d implying a long lifetime in the bare microscopic units. The decay

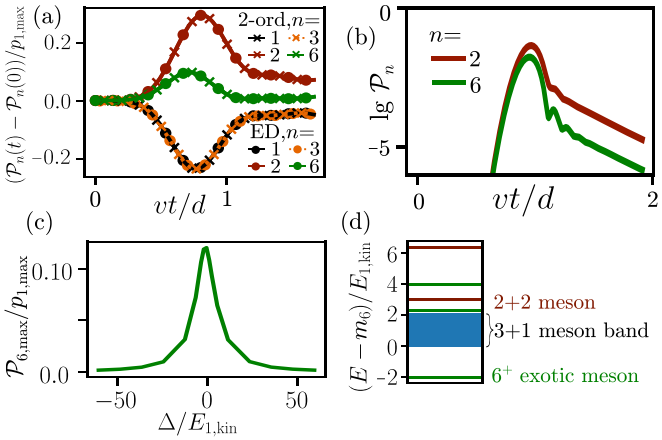

FIG. 2. Particle production in the $(3+1)$-collision for $h_z = J$, $h_x = 10^{-2}J$. (a) Normalized particle production, $[\mathcal{P}_n(t) - \mathcal{P}_n(0)]/p_{1,\max}$, comparing ED of the full Ising model to the effective theory for $L = 20$; $p_{1,\max}$ is the maximum on-site probability of the 1-meson wave packet, $v = 2h_x^2/3J$ is its group velocity, and $d = L/2$ is the initial distance between the centers of 3- and 1-mesons. (b) Dynamics of the 2- and 6-meson occupations for $L = 100$ calculated for the effective model. (c) Maximum production of the intermediate states vs detuning Δ, Eq. (7), normalized by the kinetic energy $E_{1,\text{kin}}$ of the 1-meson. (d) Spectrum in the vicinity of the exotic 6^+-meson.

of such high-energy particles aligns with general expectations of string breaking where heavy mesons with a large string tension decay at the expense of creating new lighter particles [22,23].

Until now we used $h_z = J$ to achieve a resonance based on an estimate of the bare rest masses leading to the natural question of what happens upon detuning the system out of this resonance. In Fig. 2(c) we show the dependence of the particle production of the 6-meson as a function of the detuning of the energy barrier

$$\Delta = m_6 - m_1 - m_3 = 4(h_z - J) - \frac{1}{3}\frac{h_x^2}{J}. \tag{7}$$

One can identify a Lorentzian-type resonance peak expected from conventional collision processes.

To understand why the inelastic channel is not more effective in creating a larger production of, e.g., the 6-mesons, it is instructive to study the full many-body spectrum. Figure 2(d) shows the energy levels of H_{eff}, Eq. (2), diagonalized in the zero-momentum sector. We see that interactions induce significant modifications with the 6-meson evolving into three exotic meson states 6^+; see the green lines in Fig. 2(d). The 6^+ states are "multiquark" bound states [37] of various n-mesons [41], which one might interpret as an analog of exotic mesons such as the tetraquarks in QCD [46]. Here, we use the notation $6^+ = 6 + 1 \otimes 3 + 2 \otimes 2$ to denote a state composed of a 6-meson, a product state of a 1- and a 3-meson, as well as a product state of two 2-mesons. The respective amplitudes are given in [41]. Importantly, the 6^+ exotic mesons are pushed out of the continuum made up of $(1+3)$-mesons, which contains the projectiles before the collision event. Therefore, the transition to the 6- and $(2+2)$-meson states becomes slightly off-resonant, which provides an

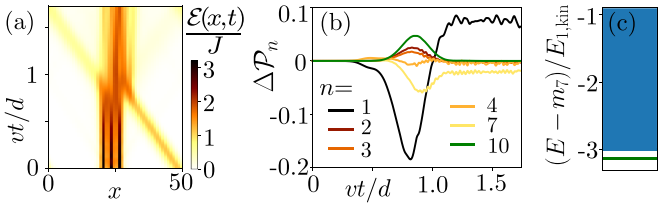

FIG. 3. Inelastic collision between the exotic 7^+-meson state and a 1-meson. (a) Spatiotemporal profile of the local energy $\mathcal{E}(x,t)$. (b) Change of the meson occupation $\Delta\mathcal{P}_n(t) = \mathcal{P}_n^{\mathrm{coll}}(t) - \mathcal{P}_n^{7^+}(t) - \mathcal{P}_n^{1}(t)$ due to the collision; here $\mathcal{P}^{7^+}$ and $\mathcal{P}^{1}$ correspond to single 7^+- and 1-meson, respectively, while P^{coll} corresponds to 7^+ and 1 collision. (c) Zoom into the many-body spectrum close to the exotic 7^+-meson in the zero-momentum sector (green). The latter is separated from the three 1-meson continuum (blue) by a small energy gap $\sim 0.1h_x^2$, which the injection of 1-meson kinetic energy allows to overcome.

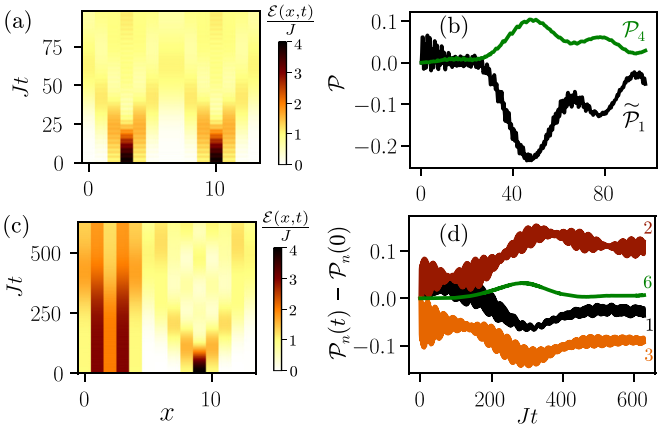

FIG. 4. Particle collisions at experimentally relevant stronger transverse fields with all mesons created by spin flips instead of wave packets as studied in the preceding sections. Upper panel: (1+1)-meson collision for $h_x/J = 1/3$. Lower panel: (3+1)-meson collision for $h_x/J = 0.15$. (a), (c) Spatiotemporal evolution of local energy $\mathcal{E}(x,t)$. (b), (d) Time dependence of the particle production: (b) dressed 1-meson projector $\tilde{\mathcal{P}}_1(t) = \mathcal{P}_1(t) + \mathcal{P}_2(t) - \mathcal{P}_1(0) - \mathcal{P}_2(0)$ and 4-meson projector $\mathcal{P}_4(t)$; (d) $\mathcal{P}_n(t) - \mathcal{P}_n(0)$ for $n = 1, 2, 3, 6$. Both collisions are studied using the full Ising Hamiltonian; the initial separation between the centers of the mesons is $d = 7, h_z = J, L = 14$.

explanation of why their respective production only reaches a value of $\mathcal{P}_n/p_1^{\max} \approx 0.1$; see Fig. 2(a).

Inelastic collision with exotic meson. We now aim to take one further step towards collisions with more complex objects. From the spectrum, Fig. 3(c), we identify another exotic meson bound state $7^+ = 7 + 1 \otimes 1 \otimes 1$ of a 7-meson with three 1-mesons [41], which is located below the continuum consisting of three 1-mesons. Crucially, the gap is small compared to the kinetic energy of an incident 1-meson, leaving us with the expectation that a collision between the exotic 7^+-meson state and a 1-meson could excite the 7^+ into the continuum 1-meson band. Figure 3(a) shows the spatiotemporal dynamics of the local energy $\mathcal{E}(x,t)$ for a setup with a 1-meson projectile impacting onto a 7^+ state. Compared to the previous inelastic collision, Fig. 1, this appears more violent, changing significantly the real-space structure. The impact of the 1-meson creates a complex transient state involving the production of many mesons of different types up to a contribution of the 10-meson [Fig. 3(b)]. After the collision, a significant weight of the initial exotic meson is indeed transformed into 1-mesons.

Towards quantum simulation of meson collisions. A key advantage of our proposed setup is that it enables a natural experimental implementation in quantum simulator platforms, which would require (i) the capability to realize the dynamics of the quantum Ising chain with sufficiently long coherence times; (ii) the preparation of the initial wave packets; and (iii) local readout capabilities for measuring $\mathcal{E}(x,t)$ and $p_n(x,t)$. In this context, systems of Rydberg atoms appear especially suitable. Since they naturally implement the targeted quantum Ising chain [26–31], the central question is how the achievable coherence times compare with the collision timescale $t^* = d/u$. The latter can be tuned via both the relative velocity u of the mesons and their initial distance d. For a $(1+1)$-collision, Figs. 4(a) and 4(b), this gives $u = 2v$, with $v = 2h_x^2/3J$ the velocity of a single 1-meson leading to $Jt^* = (3d/4)(J/h_x)^2 \approx 47$ for $d = 7$ and $h_x/J = 1/3$, which matches the timescales accessed recently in Ref. [34]. Systems of Rydberg atoms provide also the local control to initialize directly the static n-mesons by flipping n spins [26,28]. For the generation of propagating particles, one can just impose simple spin flips, which creates 1-mesons experiencing a simple quantum walk, Fig. 4(a). Further, the measurement outcomes in systems of Rydberg atoms are spin configurations [26–31], from whose statistics one can directly obtain the individual meson occupations as depicted in Fig. 4(b). This collision leads to the production of 4-mesons at the expense of a reduction of 1-mesons. Note that here we measure the 1-meson occupation in a slightly different way as compared to the case of weaker transverse fields studied above. The measurement of the n-mesons by the projectors $\mathcal{P}_n(t)$ is only exact in the asymptotic limit $h_x/J \to 0$ with corrections at nonzero transverse fields. For the case considered in Fig. 4(b) we find from a perturbative analysis taking into account h_x/J corrections that the 1-mesons are dressed by 2-mesons. As a consequence, we can get a better estimate $\tilde{\mathcal{P}}_1(t) = \mathcal{P}_1(t) + \mathcal{P}_2(t)$ of the actual 1-meson occupation by adding up the two bare 1- and 2-meson contributions.

In Figs. 4(c) and 4(d) we explore a $(3+1)$-meson collision analogous to the one studied in Figs. 1 and 2. Since the collision involves more types of mesons, namely 1-, 2-, 3-, and 6-meson, it becomes more important to use a smaller value of $h_x/J = 0.15$ in order to be able to neglect the dressing contributions to the mesons. Due to smaller h_x, the characteristic collision time increases to $Jt \sim 300$, which is larger by a factor of ~ 6 as compared to the timescales reached in the recent experiments [27,34]. This appears challenging, but it might be achievable in the foreseeable future.

Opportunities for the use of the method. The utilized method for the simulation of particle collisions is based on a perturbatively controlled mapping of the dynamics into a small effective subspace of the full Hilbert space. Importantly, the resulting algorithm requires only numerical resources polynomial in the system's volume, making it

very efficient. The method is controlled when operated in the large mass limit of the charges ($h_x \ll J$ in our model) and independently from the string tension (set by h_z). For LGTs, similar limits can also be taken upon considering large masses for the matter fields. Consequently, the numerical resources still scale only polynomially with the volume, which makes our approach promising for the challenge to access particle collisions in two or more space dimensions [47].

Also from an experimental point of view, the straightforward extension of our work to LGTs in higher dimensions might provide a useful tool to probe their physics via particle collisions, such as exotic meson states at higher energies. Concretely, knowledge on low-energy excitations of a specific LGT can be used to create the projectiles. Measuring the spatiotemporal collision dynamics of the local energy can, for instance, provide a direct and unbiased insight on the structure of the produced particles, such as their size and velocity. In further steps, more refined measurements on individual theoretically proposed candidate particles can be performed analogous to our n-meson operators. While there are still experimental challenges to realize such complex dynamics in higher-dimensional LGTs, quantum simulators may quickly show their strengths in accessing regimes that are beyond theory methods.

Note added. During the completion of this project, we became aware of a related work [48]. Also, after the first version of the present manuscript appeared, other related works were submitted to the arXiv [24,49,50].

Acknowledgments. Valuable discussions with Johannes Zeiher are gratefully acknowledged. Exact diagonalization was performed using the ELPA library [51,52]. We gratefully acknowledge the help provided by the support team of MPCDF in Garching and, in particular, Andreas Marek. P.K. acknowledges the support of the Alexander von Humboldt Foundation. The Gravity, Quantum Fields and Information group at the Max Planck Institute for Gravitational Physics (Albert Einstein Institute) is supported by the Alexander von Humboldt Foundation and the Federal Ministry for Education and Research through the Sofja Kovalevskaja Award. This project has received funding from the European Research Council (ERC) under the European Unions Horizon 2020 research and innovation programme (Grant Agreement No. 853443). M.H. further acknowledges support by the Deutsche Forschungsgemeinschaft via the Gottfried Wilhelm Leibniz Prize program.

[1] I. Bloch, J. Dalibard, and S. Nascimbene, Quantum simulations with ultracold quantum gases, Nat. Phys. **8**, 267 (2012).

[2] R. Blatt and C. Roos, Quantum simulations with trapped ions, Nat. Phys. **8**, 277 (2012).

[3] I. M. Georgescu, S. Ashhab, and F. Nori, Quantum simulation, Rev. Mod. Phys. **86**, 153 (2014).

[4] E. A. Martinez, C. A. Muschik, P. Schindler, D. Nigg, A. Erhard, M. Heyl, P. Hauke, M. Dalmonte, T. Monz, P. Zoller, and R. Blatt, Real-time dynamics of lattice gauge theories with a few-qubit quantum computer, Nature (London) **534**, 516 (2016).

[5] F. Görg, K. Sandholzer, J. Minguzzi, R. Desbuquois, M. Messer, and T. Esslinger, Realization of density-dependent Peierls phases to engineer quantized gauge fields coupled to ultracold matter, Nat. Phys. **15**, 1161 (2019).

[6] N. Klco, E. F. Dumitrescu, A. J. McCaskey, T. D. Morris, R. C. Pooser, M. Sanz, E. Solano, P. Lougovski, and M. J. Savage, Quantum-classical computation of Schwinger model dynamics using quantum computers, Phys. Rev. A **98**, 032331 (2018).

[7] N. Klco, M. J. Savage, and J. R. Stryker, SU(2) non-Abelian gauge field theory in one dimension on digital quantum computers, Phys. Rev. D **101**, 074512 (2020).

[8] C. Schweizer, F. Grusdt, M. Berngruber, L. Barbiero, E. Demler, N. Goldman, I. Bloch, and M. Aidelsburger, Floquet approach to Z_2 lattice gauge theories with ultracold atoms in optical lattices, Nat. Phys. **15**, 1168 (2019).

[9] B. Yang, H. Sun, R. Ott, H.-Y. Wang, T. V. Zache, J. C. Halimeh, Z.-S. Yuan, P. Hauke, and J.-W. Pan, Observation of gauge invariance in a 71-site Bose-Hubbard quantum simulator, Nature (London) **587**, 392 (2020).

[10] M. Bañuls *et al.*, Simulating lattice gauge theories within quantum technologies, Eur. Phys. J. D **74**, 165 (2020).

[11] M. Greiter, Fictitious flux confinement: Magnetic pairing in coupled spin chains or planes, Phys. Rev. B **66**, 054505 (2002).

[12] B. Lake, A. M. Tsvelik, S. Notbohm, D. Alan Tennant, T. G. Perring, M. Reehuis, C. Sekar, G. Krabbes, and B. Büchner, Confinement of fractional quantum number particles in a condensed-matter system, Nat. Phys. **6**, 50 (2010).

[13] C. M. Morris, R. Valdés Aguilar, A. Ghosh, S. M. Koohpayeh, J. Krizan, R. J. Cava, O. Tchernyshyov, T. M. McQueen, and N. P. Armitage, Hierarchy of Bound States in the One-Dimensional Ferromagnetic Ising Chain $CoNb_2O_6$ Investigated by High-Resolution Time-Domain Terahertz Spectroscopy, Phys. Rev. Lett. **112**, 137403 (2014).

[14] B. Grenier, S. Petit, V. Simonet, E. Canévet, L. P. Regnault, S. Raymond, B. Canals, C. Berthier, and P. Lejay, Longitudinal and Transverse Zeeman Ladders in the Ising-Like Chain Antiferromagnet $BaCo_2V_2O_8$, Phys. Rev. Lett. **114**, 017201 (2015).

[15] M. Kormos, M. Collura, G. Takács, and P. Calabrese, Real-time confinement following a quantum quench to a non-integrable model, Nat. Phys. **13**, 246 (2017).

[16] A. K. Bera, B. Lake, F. H. L. Essler, L. Vanderstraeten, C. Hubig, U. Schollwöck, A. T. M. N. Islam, A. Schneidewind, and D. L. Quintero-Castro, Spinon confinement in a quasi-one-dimensional anisotropic Heisenberg magnet, Phys. Rev. B **96**, 054423 (2017).

[17] P. P. Mazza, G. Perfetto, A. Lerose, M. Collura, and A. Gambassi, Suppression of transport in nondisordered quantum spin chains due to confined excitations, Phys. Rev. B **99**, 180302(R) (2019).

[18] N. J. Robinson, A. J. A. James, and R. M. Konik, Signatures of rare states and thermalization in a theory with confinement, Phys. Rev. B **99**, 195108 (2019).

[19] A. J. A. James, R. M. Konik, and N. J. Robinson, Nonthermal States Arising from Confinement in One and Two Dimensions, Phys. Rev. Lett. **122**, 130603 (2019).

[20] M. C. Bañuls, M. P. Heller, K. Jansen, J. Knaute, and V. Svensson, From spin chains to real-time thermal field theory using tensor networks, Phys. Rev. Research **2**, 033301 (2020).

[21] L. Vanderstraeten, E. Wybo, N. Chepiga, F. Verstraete, and F. Mila, Spinon confinement and deconfinement in spin-1 chains, Phys. Rev. B **101**, 115138 (2020).

[22] A. Lerose, F. M. Surace, P. P. Mazza, G. Perfetto, M. Collura, and A. Gambassi, Quasilocalized dynamics from confinement of quantum excitations, Phys. Rev. B **102**, 041118(R) (2020).

[23] R. Verdel, F. Liu, S. Whitsitt, A. V. Gorshkov, and M. Heyl, Real-time dynamics of string breaking in quantum spin chains, Phys. Rev. B **102**, 014308 (2020).

[24] A. Milsted, J. Liu, J. Preskill, and G. Vidal, Collisions of false-vacuum bubble walls in a quantum spin chain, PRX Quantum **3**, 020316 (2022).

[25] M. Van Damme, L. Vanderstraeten, J. De Nardis, J. Haegeman, and F. Verstraete, Real-time scattering of interacting quasiparticles in quantum spin chains, Phys. Rev. Research **3**, 013078 (2021).

[26] H. Bernien, S. Schwartz, A. Keesling, H. Levine, A. Omran, H. Pichler, S. Choi, A. S. Zibrov, M. Endres, M. Greiner, V. Vuletić, and M. D. Lukin, Probing many-body dynamics on a 51-atom quantum simulator, Nature (London) **551**, 579 (2017).

[27] J. Zeiher, J.-y. Choi, A. Rubio-Abadal, T. Pohl, R. van Bijnen, I. Bloch, and C. Gross, Coherent Many-Body Spin Dynamics in a Long-Range Interacting Ising Chain, Phys. Rev. X **7**, 041063 (2017).

[28] M. Marcuzzi, J. Minář, D. Barredo, S. de Léséleuc, H. Labuhn, T. Lahaye, A. Browaeys, E. Levi, and I. Lesanovsky, Facilitation Dynamics and Localization Phenomena in Rydberg Lattice Gases with Position Disorder, Phys. Rev. Lett. **118**, 063606 (2017).

[29] V. Lienhard, S. de Léséleuc, D. Barredo, T. Lahaye, A. Browaeys, M. Schuler, L.-P. Henry, and A. M. Läuchli, Observing the Space- and Time-Dependent Growth of Correlations in Dynamically Tuned Synthetic Ising Models with Antiferromagnetic Interactions, Phys. Rev. X **8**, 021070 (2018).

[30] E. Guardado-Sanchez, P. T. Brown, D. Mitra, T. Devakul, D. A. Huse, P. Schauß, and W. S. Bakr, Probing the Quench Dynamics of Antiferromagnetic Correlations in a 2D Quantum Ising Spin System, Phys. Rev. X **8**, 021069 (2018).

[31] S. de Léséleuc, S. Weber, V. Lienhard, D. Barredo, H. P. Büchler, T. Lahaye, and A. Browaeys, Accurate Mapping of Multilevel Rydberg Atoms on Interacting Spin-1/2 Particles for the Quantum Simulation of Ising Models, Phys. Rev. Lett. **120**, 113602 (2018).

[32] A. Keesling, A. Omran, H. Levine, H. Bernien, H. Pichler, S. Choi, R. Samajdar, S. Schwartz, P. Silvi, S. Sachdev, P. Zoller, M. Endres, M. Greiner, V. Vuletić, and M. D. Lukin, Quantum Kibble-Zurek mechanism and critical dynamics on a programmable Rydberg simulator, Nature (London) **568**, 207 (2019).

[33] S. Ebadi, T. T. Wang, H. Levine, A. Keesling, G. Semeghini, A. Omran, D. Bluvstein, R. Samajdar, H. Pichler, W. W. Ho, S. Choi, S. Sachdev, M. Greiner, V. Vuletić, and M. D. Lukin, Quantum phases of matter on a 256-atom programmable quantum simulator, Nature (London) **595**, 227 (2021).

[34] D. Wei, A. Rubio-Abadal, B. Ye, F. Machado, J. Kemp, K. Srakaew, S. Hollerith, J. Rui, S. Gopalakrishnan, N. Y. Yao, I. Bloch, and J. Zeiher, Quantum gas microscopy of Kardar-Parisi-Zhang superdiffusion, Science **376**, 716 (2022).

[35] See [25] for an earlier study of collisions in spin chains. The main differences are an underlying motivation with quantum simulation prospects playing a prominent role in our work and a different quantum model that allows us to have very violent inelastic collisions.

[36] B. M. McCoy and T. T. Wu, Two-dimensional Ising field theory in a magnetic field: Breakup of the cut in the two-point function, Phys. Rev. D **18**, 1259 (1978).

[37] P. Fonseca and A. Zamolodchikov, Ising Spectroscopy I: Mesons at $T < T_c$, arXiv:hep-th/0612304.

[38] S. Bravyi, D. P. DiVincenzo, and D. Loss, Schrieffer-Wolff transformation for quantum many-body systems, Ann. Phys. **326**, 27932826 (2011).

[39] A. B. Zamolodchikov, Integrals of motion and S matrix of the (scaled) T = T(c) Ising model with magnetic field, Int. J. Mod. Phys. A **04**, 4235 (1989).

[40] R. Coldea, D. A. Tennant, E. M. Wheeler, E. Wawrzynska, D. Prabhakaran, M. Telling, K. Habicht, P. Smeibidl, and K. Kiefer, Quantum criticality in an Ising chain: Experimental evidence for emergent e_8 symmetry, Science **327**, 177 (2010).

[41] See Supplemental Material at http://link.aps.org/supplemental/10.1103/PhysRevResearch.4.L032001 for details about construction of the effective perturbation theory model, exotic meson bound states, the resonances beyond $h_z = J$, the elastic collisions, the experimentally relevant collision protocol, and the schematic phase diagram of the model.

[42] T. Kinoshita, T. Wenger, and D. S. Weiss, A quantum Newton's cradle, Nature (London) **440**, 900 (2006).

[43] Y. Tang, W. Kao, K.-Y. Li, S. Seo, K. Mallayya, M. Rigol, S. Gopalakrishnan, and B. L. Lev, Thermalization Near Integrability in a Dipolar Quantum Newton's Cradle, Phys. Rev. X **8**, 021030 (2018).

[44] M. Hyrkäs, V. Apaja, and M. Manninen, Many-particle dynamics of bosons and fermions in quasi-one-dimensional flat-band lattices, Phys. Rev. A **87**, 023614 (2013).

[45] M. Mamaev, I. Kimchi, M. A. Perlin, R. M. Nandkishore, and A. M. Rey, Quantum Entropic Self-Localization with Ultracold Fermions, Phys. Rev. Lett. **123**, 130402 (2019).

[46] Y.-R. Liu, H.-X. Chen, W. Chen, X. Liu, and S.-L. Zhu, Pentaquark and Tetraquark states, Prog. Part. Nucl. Phys. **107**, 237 (2019).

[47] P. Karpov *et al.* (unpublished)

[48] F. M. Surace and A. Lerose, Scattering of mesons in quantum simulators, New J. Phys. **23**, 062001 (2021).

[49] A. Bastianello, U. Borla, and S. Moroz, Fragmentation and Emergent Integrable Transport in the Weakly Tilted Ising Chain, Phys. Rev. Lett. **128**, 196601 (2022).

[50] J. Vovrosh, R. Mukherjee, A. Bastianello, and J. Knolle, Dynamical hadron formation in long-range interacting quantum spin chains, arXiv:2204.05641 [cond-mat.quant-gas].

[51] T. Auckenthaler, V. Blum, H.-J. Bungartz, T. Huckle, R. Johanni, L. Krmer, B. Lang, H. Lederer, and P. Willems, Parallel solution of partial symmetric eigenvalue problems from electronic structure calculations, Parallel Computing **37**, 783

(2011), 6th International Workshop on Parallel Matrix Algorithms and Applications (PMAA'10).

[52] A. Marek, V. Blum, R. Johanni, V. Havu, B. Lang, T. Auckenthaler, A. Heinecke, H.-J. Bungartz, and H. Lederer, The ELPA library: scalable parallel eigenvalue solutions for electronic structure theory and computational science, J. Phys.: Condens. Matter **26**, 213201 (2014).